Tkachenko modes and structural phase transitions of the vortex lattice of a two-component Bose-Einstein condensate

M. Keçeli and M. Ö. Oktel*
Department of Physics, Bilkent University, 06800 Ankara, Turkey
(Dated: February 2, 2008)

We consider a rapidly rotating two-component Bose-Einstein condensate (BEC) containing a vortex lattice. We calculate the dispersion relation for small oscillations of vortex positions (Tkachenko modes) in the mean-field quantum Hall regime, taking into account the coupling of these modes with density excitations. Using an analytic form for the density of the vortex lattice, we numerically calculate the elastic constants for different lattice geometries. We also apply this method to calculate the elastic constant for the single-component triangular lattice. For a two-component BEC, there are two kinds of Tkachenko modes, which we call acoustic and optical in analogy with phonons. For all lattice types, acoustic Tkachenko mode frequencies have quadratic wave-number dependence at long-wavelengths, while the optical Tkachenko modes have linear dependence. For triangular lattices the dispersion of the Tkachenko modes are isotropic, while for other lattice types the dispersion relations show directional dependence consistent with the symmetry of the lattice. Depending on the intercomponent interaction there are five distinct lattice types, and four structural phase transitions between them. Two of these transitions are second-order and are accompanied by the softening of an acoustic Tkachenko mode. The remaining two transitions are first-order and while one of them is accompanied by the softening of an optical mode, the other does not have any dramatic effect on the Tkachenko spectrum. We also find an instability of the vortex lattice when the intercomponent repulsion becomes stronger than the repulsion within components.

PACS numbers: 03.75.Lm,03.75.Mn,03.75.Kk,67.40.Db

I. INTRODUCTION

One of the defining properties of superfluidity is that a superfluid responds to rotation by forming quantized vortices. Generally, instead of forming multiply quantized vortices, it is more favorable for a superfluid to create many singly quantized vortices and arrange them in a vortex lattice. Since the original predication of such structures by Abrikosov [1], vortex lattices have been observed in type-II superconductors [2], superfluid helium [3], Bose-Einstein condensed gases (BECs) [4, 5] and most recently in ultracold fermion superfluids[6].

Once a vortex lattice is formed in a superfluid, small deviations of the vortices from their equilibrium positions require relatively small energy compared to other hydrodynamic modes of the system, and collective behavior of such small deviations result in a low-energy branch in the excitation spectrum. The modes on this branch, which were studied by Tkachenko in the context of superfluid helium [7], are called Tkachenko modes and in a simplified picture can be thought of as phonons of the vortex lattice. Tkachenko modes strongly affect the dynamics of the superfluid [8], and play an important role in many different problems, ranging from vortex melting [9] to neutron star glitches [10].

Recent experiments on ultracold atoms have been successful in creating large vortex lattices in rotating harmonically trapped BECs [4, 5]. Remarkable results about vortex dynamics have been obtained, including the observation of Tkachenko modes over a large range of rotation frequencies [11]. In this experiment, after the formation of the vortex lattice, a resonant laser beam was focused on the center of the condensate to excite the Tkachenko modes and subsequently their frequency was measured. As the rotation frequency is increased, a clear reduction in the Tkachenko mode frequencies is observed.

Theoretical study of Tkachenko modes of trapped BECs has been carried out by a number of groups [12, 13, 14, 15, 16, 17, 18, 19]. In particular, the effects of finite size of the vortex lattice and the compressibility of the BEC lead to major differences in the Tkachenko spectrum compared with the Tkachenko modes of an incompressible superfluid such as helium. As the rotation frequency of the cloud is increased, the compressibility of the BEC starts to play an important role, reducing the shear modulus of the vortex lattice and thus the Tkachenko mode frequencies. When the rotation frequency Ω becomes close to the chemical potential $\mu = gn$, the gas enters the mean-field quantum Hall

*Electronic address: oktel@fen.bilkent.edu.tr

regime [20] where only the states in the lowest Landau level (LLL) are populated. Here, the trend of decrease in Tkachenko frequencies continues. As the rotation frequency Ω gets closer to the trapping frequency ω, more vortices enter the system, and mean-field description breaks down at the point where the number of vortices is comparable to the number of particles [9]. In the strongly correlated regime, the vortex lattice is expected to melt into a vortex liquid and subsequently go through a sequence of quantum Hall states ending with the Bosonic Laughlin state when $(\omega - \Omega)/\omega \sim 1/N$, with N being the number of particles [21].

In the experiments of the JILA group, rotation frequencies up to 99% of the trapping frequency have been achieved [22] and a calculation of the Tkachenko frequencies in the mean-field quantum Hall regime [13] found good agreement with the observed frequencies. However, a number of papers have since argued that this calculation uses an incorrect value for the shear modulus of the vortex lattice [14, 15]. When the recalculated value of the shear modulus, which is an order of magnitude higher, is used, the experimental results seem to indicate that the gas is not in the LLL regime. Although in this paper we mainly consider two-component BECs, our method is applicable to the single-component lattice, and our calculations are in excellent agreement with the latter value for the shear modulus, suggested by Sonin [14].

The versatility of the trapped cold atom experiments have enabled the creation of new superfluids, such as mixtures and spinor condensates. In a remarkable experiment the JILA group has been able to create a two-component BEC and study its behavior under rotation [23]. The equilibrium vortex lattice structures have been calculated by Mueller and Ho [24], and separately by Kasamatsu, Tsubota, and Ueda [25]. Experimentally, an interlaced square lattice of two-components has been observed. Furthermore, using an excitation procedure similar to the one-component case, vortex lattice oscillations have been induced in the two-component BEC, however, these excitations were found to be heavily damped and have not yielded a measurement for Tkachenko frequencies. Motivated by this experiment, in this paper, we calculate the Tkachenko modes of a two-component vortex lattice, and investigate the structural phase transitions between different lattice geometries.

We consider a large two-component vortex lattice in the LLL regime. To simplify the calculations, we assume that both components have the same density and same scattering length within each component. As the scattering length between atoms from different components is varied, the vortex lattice goes through structural phase transitions, forming five different lattice geometries [24]. For all these lattice geometries, we calculate the elastic constants of the vortex lattice, and subsequently the dispersion relations for long-wavelength Tkachenko modes. Our main results are summarized below.

Unlike a single-component vortex lattice, where there is only one branch of Tkachenko modes, the two-component lattice has two branches. The situation is similar to phonon modes of a diatomic solid compared with a monoatomic solid. When the number of atoms per unit cell is doubled, so are the number of phonon modes. In analogy with phonons, we call these branches acoustic Tkachenko modes, and optical Tkachenko modes. However, these names are not intended to imply that one branch couples more strongly to light than sound, or vice versa. As a simple picture, one may think that when an acoustic mode is excited two vortices inside the unit cell of the lattice oscillate in-phase. In other words, acoustic modes are oscillations of the "center of mass" of the unit cell, while the vortices positions with respect to the center of mass remain stationary. For an optical Tkachenko mode, vortices of different components oscillate in opposite phase, leaving the "center of mass" of each unit cell stationary. In this paper, we choose our interactions such that there is symmetry under the exchange of components, which makes the above definitions of optical and acoustic unambiguous. If this symmetry is broken, as is the case with the parameters of the JILA experiment, there will still be two modes, but both of them will contain a mixture of acoustic and optical behavior.

For an incompressible superfluid such as helium, or at low rotation frequencies for BEC, Tkachenko modes in a single-component vortex lattice have linear wave-vector dependence $\omega_T \propto k$ [8]. However, when compressibility of the fluid becomes important, such as a BEC in the LLL, Tkachenko modes are quadratic in the wave-vector $\omega_T \propto k^2$ [13]. We find that a similar softening happens for the two-component vortex lattice. For an incompressible fluid, acoustic Tkachenko modes have linear long-wavelength behavior, while the optical Tkachenko modes are gapped. For a two-component BEC in the LLL, acoustic Tkachenko modes have quadratic wave-vector dependence $\omega_T^{\rm ac} \propto k^2$, while the optical modes are not gapped any more, but have linear wave-vector dependence $\omega_T^{\rm op} \propto k$.

Another important property of the Tkachenko modes of a single-component system is their isotropy. Tkachenko mode frequencies are independent of the direction of the excitation wave vector $\vec{k}$. This can be traced back to the fact that the underlying vortex lattice is triangular, and similar to acoustic waves in a triangular lattice, Tkachenko modes have isotropic behavior [26]. For two-component vortex lattices, this behavior is not expected any more, and indeed we find that when the underlying lattice has less than sixfold symmetry, both acoustic and optical Tkachenko modes are anisotropic. In all cases the anisotropy reflects the reduced symmetry of the lattice, giving fourfold symmetric dispersion relations for the square lattice, and twofold symmetric spectra for rhombic and rectangular lattices.

Another interesting point about the two-component vortex lattices is the possibility of structural phase transitions between different lattice geometries. For a two-component BEC in the LLL there are five lattice structures and four

structural phase transitions between them. Two of these are continuous, second-order transitions, while the other two are first-order transitions. In structural phase transitions of solids, second-order phase transitions are signalled by the softening of an acoustic-phonon mode, while first-order transitions are usually, but not always, accompanied by the softening of an optical-phonon mode. (A soft mode can be described as a branch of excitation that has zero frequency over a large range of wave vectors [27].) We find that a similar scenario plays out for the vortex lattices of two-component BECs, both second-order phase transitions have a soft acoustic Tkachenko mode. Of the two first-order phase transitions, one is accompanied by a soft optical Tkachenko mode, while the other does not have a direct effect on the long-wavelength Tkachenko spectrum of the system.

There are two other instabilities in the two-component BEC system. When the intercomponent attraction is stronger than the repulsion within each component, the gas is unstable towards collapse. In the opposite limit, when the intercomponent interaction is repulsive and stronger than the intracomponent repulsion we find an instability in the optical Tkachenko mode spectrum, most possibly signaling a transition to a phase separated state.

The paper is organized as follows. In the next section, we introduce the Hamiltonian for the two-component rotating gas in the LLL, and introduce the different lattice types that are found by energy minimization. In Sec. III, we outline our method of calculation for elastic coefficients, and calculate the shear modulus of a one-component condensate as an example. In Sec. IV, we write the coupled equations for the vortex modes and density modes, which are valid for all lattice types. In the next five sections V -IX, we calculate the elastic energy for each lattice type, and by solving the coupled equations, we find the dispersion relations of acoustic and optical Tkachenko modes. We also study the directional dependence of the dispersion relations and the polarization of the Tkachenko modes for each lattice type. In Sec. X, we discuss the structural phase transitions and identify the soft modes associated with each transition. Finally, in Sec. XI, we summarize our results and discuss their consequences for experiments.

II. VORTEX LATTICES OF TWO-COMPONENT BEC

In this section, we consider the equilibrium vortex lattice configurations of a two-component BEC. This problem has been studied in the LLL regime analytically by Mueller and Ho [24], and for general rotation frequencies numerically by Kasamatsu *et al.* [25]. We confine ourselves to the LLL and our method of calculation of the elastic constants relies on the analytic approach developed by Mueller and Ho.

We consider a two-component BEC in a quadratic trap with trapping frequency ω. The trap frequency, the mass of the particles m, and the total number of particles are assumed to be the same for both components. We take the gas to be rotating at frequency Ω, and assume that the total number of particles in each component is large enough to form a large vortex lattice without a breakdown of the mean-field description of the system. Furthermore, we assume that the scattering lengths of the particles are such that, interaction parameters satisfy

$$\begin{aligned} g_{11} &= g_{22} = g, \\ g_{12} &= \alpha g. \end{aligned} \tag{1}$$

We investigate the behavior of vortex lattice geometry and the Tkachenko modes as the ratio of intercomponent scattering length to intracomponent scattering length α is varied,

$$\alpha = \frac{g_{12}}{g}. \tag{2}$$

We limit our discussion of vortex lattices to two dimensions, assuming that the vortex lattice is not modified along the rotation axis. This assumption is not very restrictive, as it has been shown that if the cloud is sufficiently broad in the third dimension, vortex bending is negligible except at the edges of the cloud [20]. In the opposite limit of a two-dimensional condensate, our approach is formally valid, however, mean-field theory may not be reliable for such a system. The energy functional for our system can be written as

$$E = \sum_{i=1,2} \int d^2 r \Psi_i^*(r) \left(-\frac{\hbar^2}{2m} \nabla^2 + \frac{1}{2} m\omega^2 r^2 - \Omega L_z \right) \Psi_i(r) + V_{\rm int}. \tag{3}$$

Here Ψ_i is the wave function of component i, L_z is the angular momentum along the rotation direction and $V_{\rm int}$ is the interaction energy given as

$$V_{\rm int} = g \int d^2 r \left(\frac{1}{2} \left[|\Psi_1(r)|^4 + |\Psi_2(r)|^4 \right] + \alpha |\Psi_1(r)|^2 |\Psi_2(r)|^2 \right). \tag{4}$$

When the rotation frequency is close enough to the trapping frequency the particles can only populate levels in the LLL. For such a gas, which is in the mean-field quantum Hall regime, the wave functions have the form

$$\Psi_i(r) = f_i(z) e^{-\frac{z\bar{z}}{2\sigma^2}}, \tag{5}$$

where $z = x + iy$ and σ is the radius of the cloud. The requirement of analyticity on the wave function essentially determines the form of the wave function in terms of the positions of the vortices (up to an entire function with no zeros). Thus it is possible to introduce a variational wave function, using just the lattice basis vectors as variational parameters.

For a two-component BEC, when both of the components are rotating at the same frequency, vortex lattices in each component have the same lattice structure, but are shifted from each other. Thus in the LLL, we can determine the wave functions for both components in terms of just three, two-dimensional vectors $\vec{a}_1$ and $\vec{a}_2$, the basis vectors of the lattice, and $\vec{d}$, the offset between the two lattices. Thus the vortices of the first component are at $\vec{r}_{1,n,m} = n\vec{a}_1 + m\vec{a}_2$, with n, m integers, while the vortices of the second component are at $\vec{r}_{2,n,m} = n\vec{a}_1 + m\vec{a}_2 + \vec{d}$. Although we need six real numbers to describe these three vectors, the actual number of variational parameters is lower, namely 4. First of all, the vortex density ν_c^{-1} is fixed by rotation frequency Ω, thus it is possible to fix the length of one of the vectors and scale all others by this length. Second, the rotational symmetry of the problem permits one to fix the overall orientation of the vectors. We choose the first lattice basis vector $\vec{a}_1$ to lie along the $\hat{x}$ direction, and denote its length as a_1. The remaining two vectors can then be written as

$$\begin{aligned} \vec{a}_2 &= a_1(u\hat{x} + v\hat{y}), \\ \vec{d} &= a_1[(a + bu)\hat{x} + bv\hat{y}]. \end{aligned} \tag{6}$$

The variational calculation is made in terms of the dimensionless parameters u, v, a, b, and then the length a_1 is fixed by requiring the wave function to have correct density of vortices $\nu_c = a_1^2 v$.

Once the positions of the vortices are known one can write the variational wave function as a Jacobi Elliptic function Θ, or as one of the doubly periodic functions that are related to the Θ up to an entire function, such as the σ function or the modified ζ function [7]. In terms of the Jacobi theta function we can write

$$\begin{aligned} \Psi_1(z) &= N_1 \Theta(\zeta, \tau) \exp(\frac{\pi z^2}{2\nu_c} - \frac{z\bar{z}}{2l}), \\ \Psi_2(z) &= N_2 \Theta(\zeta - (a + bu + ibv), \tau) \exp(\frac{\pi z^2}{2\nu_c} - \frac{z\bar{z}}{2l}). \end{aligned} \tag{7}$$

Here $\zeta = z/a_1$, $\tau = u + iv$, $l = \sqrt{\hbar/m\omega}$, and N_1, N_2 are normalization constants to be determined. With these wave functions we calculate the densities of the two-components as

$$\begin{aligned} |\Psi_1(\vec{r})|^2 &= C g(\vec{r}) e^{-r^2/\sigma^2}, \\ |\Psi_2(\vec{r})|^2 &= C g(\vec{r} - \vec{d}) e^{-r^2/\sigma^2}, \end{aligned} \tag{8}$$

where the function g is periodic with lattice vectors,

$$g(\vec{r} + n\vec{a_1} + m\vec{a_2}) = g(\vec{r}), \tag{9}$$

for all integers n, m. The periodic part of the density admits a Fourier series representation in terms of the reciprocal-lattice basis vectors,

$$g(\vec{r}) = \frac{1}{\nu_c} \sum_{\vec{K}} g_{\vec{K}} e^{i\vec{r}\cdot\vec{K}}, \tag{10}$$

with the sum carried out over all reciprocal lattice points generated by $\vec{K}_1 = \frac{2\pi}{\nu_c}\vec{a}_2 \times \hat{z}$ and $\vec{K}_2 = -\frac{2\pi}{\nu_c}\vec{a}_1 \times \hat{z}$. The utility of using the Jacobi theta function is that the Fourier components of $g_{\vec{K}}$ can be calculated with relative ease. For $\vec{K} = m_1\vec{K}_1 + m_2\vec{K}_2$ one has

$$g_{\vec{K}} = (-1)^{m_1 + m_2 + m_1 m_2} e^{-\frac{\nu_c \vec{K}^2}{8\pi}} \sqrt{\frac{\nu_c}{2}}. \tag{11}$$

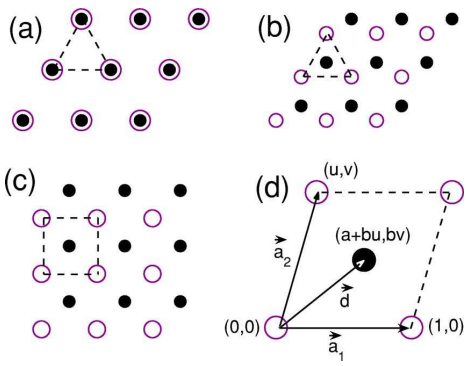

FIG. 1: Lattice geometry for an overlapped triangular lattice (a), an interlaced triangular lattice (b), and a square lattice (c). Unit cells are shown with dashed lines. (d) Unit cell geometry for an arbitrary lattice. White and black dots represent vortices of different components. Definitions of a, b, u, v are given in Sec. II.

In the LLL, the lattice structure is entirely determined by the interaction energy. For the parameters used here minimization of the interaction energy reduces to a minimization of the following simple quantity with respect to u, v, a, and b:

$$J = \sum_{\vec{K}} \left| \frac{g_{\vec{K}}}{g_{\vec{0}}} \right|^2 \left(1 + \alpha \cos(\vec{K} \cdot \vec{d}) \right). \tag{12}$$

It must be noted that this expression is obtained in the limit of a very large vortex lattice, formally setting the cloud radius σ to infinity. The minimization of J is done numerically with considerable ease as the Fourier coefficients of the density $g_{\vec{K}}$ are known analytically. For each value of $\alpha = g_{12}/g$, J can be calculated by truncating the rapidly converging sum to the desired accuracy, and the values u_*, v_*, a_*, b_* that minimize J can be found. These values determine the lattice geometry for each component and also the offset of the lattices of two-components.

As the ratio of the intercomponent interaction to intracomponent interaction α is varied, five different lattice types are found to minimize the interaction energy. Here, we give a brief description of each lattice, and in Secs. V - IX, the Tkachenko spectrum for each lattice type is calculated.

When the interaction between the two-components is attractive, i.e., $\alpha < 0$, the system minimizes its energy by positioning the vortex lattices of two-components on top of each other. However, for very large attraction, $\alpha < -1$, there is an instability towards collapse. In the range $-1 < \alpha < 0$, both components form triangular lattices which overlap with each other (See fig. 1). This overlapped triangular lattice is described by the parameters $u_* = 1/2, v_* = \sqrt{3}/2, a_* = b_* = 0$, which do not change with α in the given range. We find, however, that the elastic constants of the lattice depend on α, and so do the Tkachenko modes.

If the intercomponent interaction becomes repulsive, it is no more favorable to put the two vortex lattices on top of each other. Instead, the most favorable places to put the vortices of one-component would be the density maxima of the other component. This simple insight holds true for all lattice types found by the minimization procedure, however the lattice type of each component changes as α is varied. For weak repulsion between the components, $0 < \alpha < 0.1724$, each component forms a triangular lattice. Within a unit cell, there is more than one density maximum, so it would seem that there are multiple positions for the vortex lattice of the second component to be placed. However, these positions are related with the overall symmetry of the lattice, so the minimization procedure gives the lattice parameters $u_* = 1/2, v_* = \sqrt{3}/2, a_* = b_* = 1/3$. Again, the overall structure of this interlaced triangular lattice (see Fig. 1) does not change with α. At $\alpha = 0.1724$, there is a first-order phase transition from an interlaced triangular lattice to a rhombic lattice. In the range $0.1724 < \alpha < 0.3733$, the unit cell of vortex lattices of each component are rhombuses. The vortex lattice of one-component is placed at the center of the rhombuses formed by the vortex lattice of the other component. The angle of the rhombus η (see Fig. 2), varies continuously from 67.9° to 90°, while the offset remains the same, $a_* = b_* = 1/2$. At $\alpha = 0.3733$, there is a second-order phase transition to a square lattice. In the range $0.3733 < \alpha < 0.9256$, the lattice is parametrized by $u_* = 0, v_* = 1, a_* = b_* = 1/2$ (see Fig. 2). As the interaction is increased further, there is a second-order phase transition to a rectangular lattice at $\alpha = 0.9256$. In a rectangular lattice, vortices of one-component are always found at the centers of the rectangles formed by the vortices of the other component, i.e., $a_* = b_* = 1/2$. However, the aspect ratio of the rectangle increases continuously.

For a nonrotating system, there is a phase-separation instability at $\alpha = 1$. This instability is not found in the results of the energy minimization described above. However, when the coupling between the density oscillations and

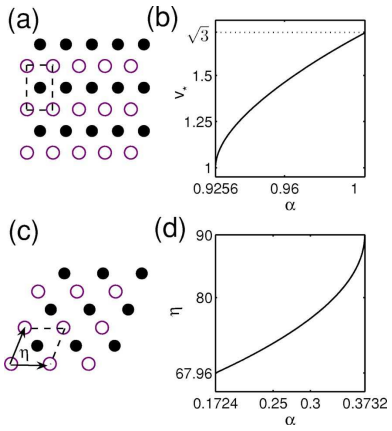

FIG. 2: (a) Lattice geometry for a rectangular lattice; a unit cell is shown with dashed lines. (b) Change of the aspect ratio of the rectangle v_* with respect to interaction strength α. The unit cell grows in the y direction as $\alpha \to 1$. At $\alpha = 1$, $v_* = \sqrt{3}$. (c) Lattice geometry of a rhombic lattice, dashed lines showing a unit cell. η is twice the opening angle of the rhombic unit cell. (d) Plot of η vs α for the rhombic lattice. As $\alpha \to 0.3732$, $\eta \to 90^\circ$, and the rhombus continuously changes to a square. At $\alpha = 0.1724$, η makes a jump from 60° to 67.958°.

vortex motion is taken into account, as in Sec. VIII, it is found that at this point there is an instability. Thus the system is not described by a vortex lattice beyond $\alpha = 1$.

After a survey of the possible lattice structures and the analytic method that is used to find these structures, in the next section we describe how the same analytic approach can be used to calculate the elastic constants of the discussed vortex lattices.

III. NUMERICAL CALCULATION OF ELASTIC CONSTANTS

The power of the analytic approach introduced in the previous section is that it can also be used to calculate the energies of lattice structures which are slightly deformed from the minimum-energy configuration. As the numerical calculation of the energy for a given lattice is quite simple, it is possible to evaluate the energy for configurations where lattice parameters have small deviations from their minimum-energy values. Such small deviations can also be described by a hydrodynamic approach. Assuming that the lattice deformations are sufficiently smooth, the vortex lattice can be treated as an elastic medium. The form of the elastic energy is constrained by symmetries of the lattice, and for small deformations, can always be taken as quadratic in displacements. Thus the long-wavelength behavior of the lattice is described by an elastic energy that is quadratic in the vortex displacement field, and the problem reduces to the calculation of the elastic constants, which are the coefficients of the quadratic terms in vortex displacements.

Our approach is to numerically calculate the energy of the vortex lattice close to the equilibrium position, and then find the elastic coefficients of the vortex lattice by making quadratic fits to the calculated energy. As a demonstration of this method, we first calculate the shear modulus of the triangular lattice of a one-component BEC. A vortex lattice in a one-component BEC is parametrized by two two-dimensional vectors $\vec{a}_1, \vec{a}_2$, the lattice basis vectors. The lattice basis vectors define the equilibrium positions of the vortices, and we denote the deviation of the vortex at lattice site n, m, from its equilibrium by the vector $\vec{\epsilon}_{n,m}$. So the position of the vortex $\vec{r}_{n,m}$ is

$$\vec{r}_{n,m} = n\vec{a}_1 + m\vec{a}_2 + \vec{\epsilon}_{n,m}. \tag{13}$$

If the vortex displacements are sufficiently smooth over large length scales, one can describe a long-wavelength vortex displacement field $\vec{\epsilon}(x, y) = \epsilon_x(x, y)\hat{x} + \epsilon_y(x, y)\hat{y}$ by a suitable coarse-graining procedure. For a triangular lattice, the elastic energy density can then be written as

$$\varepsilon_{\text{elastic}} = C_1 \left(\frac{\partial \epsilon_x}{\partial x} + \frac{\partial \epsilon_y}{\partial y} \right)^2 + C_2 \left[\left(\frac{\partial \epsilon_x}{\partial x} - \frac{\partial \epsilon_y}{\partial y} \right)^2 + \left(\frac{\partial \epsilon_x}{\partial y} + \frac{\partial \epsilon_y}{\partial x} \right)^2 \right]. \tag{14}$$

For a gas in the LLL, compression modulus is zero, $C_1 = 0$ [8]. Using the analytic method introduced above, the shear modulus C_2 is determined as follows.

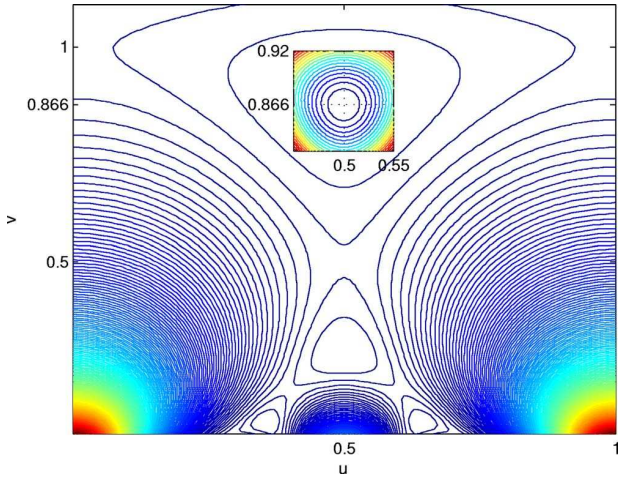

FIG. 3: Contour plot of the energy for a one-component triangular lattice, Eq. (15). The inset is a closer view around the equilibrium point. Circular contours indicate that quadratic fit of Eq. (16) is possible.

For a one-component vortex lattice, the minimum-energy configuration is found by minimizing

$$I = \sum_{\vec{K}} \left| \frac{g_{\vec{K}}}{g_{\vec{0}}} \right|^2 , \tag{15}$$

and yields $u_* = 1/2, v_* = \sqrt{3}/2$, the triangular lattice. We calculate the energy around this point by varying u and v from their equilibrium values. A contour plot of the energy around the equilibrium point is given in Fig. 3. To this form we can successfully fit a quadratic form, giving us an elastic energy of the form

$$E_{\text{elastic}} = \frac{gn^2}{2} \left[C_u (u-u_*)^2 + C_v (v-v_*)^2 + C_{uv} (u-u_*)(v-v_*) \right] , \tag{16}$$

and determine

$$\begin{aligned} C_u &= 0.3177, \\ C_v &= 0.3177, \\ C_{uv} &= 0.000. \end{aligned} \tag{17}$$

The fact that $C_u = C_v$ shows that there is only one shear modulus for a triangular lattice, and validates our numerical procedure. To find the connection between C_u and the shear modulus C_2, we must determine the displacement field corresponding to small changes of the lattice basis vectors. By taking into account that the unit-cell volume is fixed by rotational frequency, the correspondence between u, v and vortex displacement field is found as

$$\begin{aligned} \frac{\partial \epsilon_x}{\partial y} &= \frac{u-u_*}{v_*}, \qquad \frac{\partial \epsilon_x}{\partial x} = -\frac{v-v_*}{2v_*}, \\ \frac{\partial \epsilon_x}{\partial y} &= \frac{v-v_*}{2v_*}, \qquad \frac{\partial \epsilon_x}{\partial y} = 0. \end{aligned} \tag{18}$$

By substituting these expressions in Eq. (14), using $u_* = 1/2, v_* = \sqrt{3}/2$ and comparing with Eq. (16) we obtain

$$C_2 = \frac{3}{8} C_u = 0.1191 gn^2. \tag{19}$$

This value is an order of magnitude larger than the value used by Baym [13], and is in excellent agreement with Sonin [14]. This is not surprising, as our method of obtaining the shear modulus is equivalent to the deformation of the lattice used by Sonin. However, the simplicity of our numerical method enables us to calculate the elastic coefficients of more complex lattices, such as the two-component lattices discussed in this paper.

For a two-component lattice, the energy of the lattice depends not only on the lattice basis vectors, but also on the offset of two lattices from each other. Hence there are four variational parameters u, v, a, b. Elastic energy around the

minimum-energy point has to be expressed as a quadratic form in all of these variables. We numerically calculate the energy of the lattice for many points around the minimum-energy point and then express the elastic energy by fitting to a form

$$E_{\rm elastic} = \frac{gn^2}{2}\left[C_u(u-u_*)^2 + C_v(v-v_*)^2 + C_{uv}(u-u_*)(v-v_*) + C_a(a-a_*)^2 + C_b(b-b_*)^2 + C_{ab}(a-a_*)(b-b_*)\right]. \tag{20}$$

Here, due to the symmetry between component 1 and component 2, it is not necessary to include terms that mix displacements a, b with deformations of the lattice u, v. This is essentially the decoupling of optical Tkachenko modes from acoustic Tkachenko modes as discussed in Sec. I.

In the next section, we give the hydrodynamic equations for a two-component condensate, but leave the form of the elastic energy unspecified. In the following sections, the form of the elastic energy and the values of the elastic constants are given separately for each lattice type. After the elastic energy is specified, hydrodynamic equations are solved and the dispersion relations for Tkachenko modes are obtained.

IV. HYDRODYNAMIC EQUATIONS

The oscillations of vortices about their equilibrium positions can be described by a hydrodynamic theory by treating the vortex lattice as an elastic medium. For trapped BECs it is important to take into account the compressibility of the gas, as the vortex lattice oscillations are coupled to density oscillations in a nontrivial way. The superfluid hydrodynamics that takes this effect into account has been developed by a number of groups in the context of superfluid He [8], and more recently applied to rotating BECs by Baym [13]. Here we describe the hydrodynamics of a two-component vortex lattice by generalizing this hydrodynamics to a two-component BEC.

As the hydrodynamic variables, we use the densities of each component $n_i(\vec{r},t)$, corresponding velocity fields $\vec{v}_i(\vec{r},t)$, and the vortex displacement fields $\vec{\epsilon}_i(\vec{r},t)$ introduced in the previous section. Here $i = 1, 2$ is component index, giving us a total of six hydrodynamic fields. However, not all of these fields are independent, as is apparent in the calculation below. We also set $\hbar = 1$ in the calculation for convenience.

The long-wavelength average of the velocity field is not irrotational, but is linked to the compressions of the vortex lattice,

$$\vec{\nabla}\times\vec{v}_i = -2\Omega\vec{\nabla}\cdot\vec{\epsilon}_i, \qquad i = 1, 2. \tag{21}$$

Similarly the superfluid acceleration equation holds for each component

$$m\left(\frac{\partial\vec{v}_i}{\partial t} + 2\vec{\Omega}\times\frac{\partial\vec{\epsilon}_i}{\partial t}\right) = -\vec{\nabla}\mu_i, \qquad i = 1, 2. \tag{22}$$

Here μ_i is the chemical potential of component i. Below we leave the index i unspecified to indicate that the equation is valid for both components.

The conservation of particle number results in the continuity equation

$$\frac{\partial n_i}{\partial t} + \vec{\nabla}\cdot(n_i\vec{v}_i) = 0, \tag{23}$$

while momentum conservation gives

$$m\left(n_i\frac{\partial\vec{v}_i}{\partial t} + 2n_i\vec{\Omega}\times\vec{v}_i\right) + \vec{\nabla}P_i = -\vec{\sigma}_i. \tag{24}$$

Here P_i is the pressure, related to the chemical potential as $\vec{\nabla}P_i = n_i\vec{\nabla}\mu_i$, and for a weakly interacting two-component condensate satisfies

$$\begin{aligned}\vec{\nabla}P_1 &= gn\vec{\nabla}n_1 + \alpha gn\vec{\nabla}n_2,\\ \vec{\nabla}P_2 &= gn\vec{\nabla}n_2 + \alpha gn\vec{\nabla}n_1.\end{aligned} \tag{25}$$

The stress vectors σ_i are obtained by taking the functional derivative of the elastic energy with respect to vortex displacement fields, as in elasticity theory,

$$\vec{\sigma}_i = \frac{\delta E_{\rm elastic}}{\delta\vec{\epsilon}_i}. \tag{26}$$

Using Eqs. (24) and (21), we have

$$2m\vec{\Omega}\times\left(\frac{\partial\vec{\epsilon_i}}{\partial t}-\vec{v}_i\right)=\frac{\vec{\sigma}_i}{n}. \tag{27}$$

The curl and divergence of these equations lead to

$$\vec{\nabla}\cdot\left(\frac{\partial\vec{\epsilon_i}}{\partial t}-\vec{v}_i\right)=\frac{\vec{\nabla}\times\vec{\sigma}_i}{2\Omega nm}, \tag{28}$$

and

$$\vec{\nabla}\times\frac{\partial\vec{\epsilon}}{\partial t}+2\Omega\vec{\nabla}\cdot\vec{\epsilon}_i=-\frac{\vec{\nabla}\cdot\vec{\sigma}_i}{2\Omega nm}. \tag{29}$$

Similarly, the divergence of the superfluid acceleration equation gives

$$\begin{aligned}\left(-\frac{\partial^2}{\partial t^2}+\frac{gn}{m}\nabla^2\right)n_1+\alpha\frac{gn}{m}\nabla^2 n_2 &= 2\Omega n\vec{\nabla}\times\frac{\partial\vec{\epsilon_1}}{\partial t},\\ \left(-\frac{\partial^2}{\partial t^2}+\frac{gn}{m}\nabla^2\right)n_2+\alpha\frac{gn}{m}\nabla^2 n_1 &= 2\Omega n\vec{\nabla}\times\frac{\partial\vec{\epsilon_2}}{\partial t}.\end{aligned} \tag{30}$$

At this stage it is preferable to take advantage of the symmetry of the equations under the exchange of component 1 with component 2. We define the symmetric and antisymmetric variables as

$$\begin{aligned}n_+ &= n_1+n_2, \qquad \vec{\epsilon}_+=\vec{\epsilon}_1+\vec{\epsilon}_2, \qquad \vec{\sigma}_+=\vec{\sigma}_1+\vec{\sigma}_2,\\ n_- &= n_1-n_2, \qquad \vec{\epsilon}_-=\vec{\epsilon}_1-\vec{\epsilon}_2, \qquad \vec{\sigma}_-=\vec{\sigma}_1-\vec{\sigma}_2.\end{aligned} \tag{31}$$

In terms of these variables we obtain two sets of three equations, where each set is decoupled from the other. The polarization of the Tkachenko modes are controlled by the polarization equation

$$\vec{\nabla}\times\frac{\partial\vec{\epsilon}_\pm}{\partial t}+2\Omega\vec{\nabla}\cdot\vec{\epsilon}_\pm=-\frac{1}{2mn\Omega}\vec{\nabla}\cdot\vec{\sigma}_\pm. \tag{32}$$

The usual sound mode equations for a two-component fluid are modified by the dynamics of the vortex lattice as

$$-\frac{\partial^2 n_\pm}{\partial t^2}+(1\pm\alpha)\frac{gn}{m}\nabla^2 n_\pm=2n\Omega\vec{\nabla}\times\frac{\partial\vec{\epsilon}_\pm}{\partial t}. \tag{33}$$

The dynamics of the vortex lattice and its interaction with the density modes is governed by

$$\vec{\nabla}\cdot\frac{\partial^2\vec{\epsilon}_\pm}{\partial t^2}+\frac{1}{n}\frac{\partial^2 n_\pm}{\partial t^2}=\frac{1}{2nm\Omega}\frac{\partial}{\partial t}\vec{\nabla}\times\vec{\sigma}_\pm. \tag{34}$$

Equations (32)-(34) form a linear set of six equations. However, as the stresses $\sigma_\pm$, depend only on the lattice displacements $\epsilon_\pm$, with the same sign, the three symmetric variable (+) equations are decoupled from the antisymmetric variable (−) equations. Thus the "+" set describes the acoustic Tkachenko modes and their coupling with the "in-phase" sound mode, while the "−" set describes the optical Tkachenko modes and their coupling to the "out-of-phase" sound mode.

In the following sections, we specify the elastic energy $E_{\rm elastic}$ for each lattice type, and calculate the dispersion relations of both acoustic and optical Tkachenko modes. Each section starts with a brief description of the properties of the lattice type under consideration. Subsequently we give the form of the elastic energy for this lattice type and the values of the numerically calculated elastic constants. We then outline the solutions of the Tkachenko mode equations Eqs. (32)-(34), for the specific form of the elastic energy, and derive the dispersion relations of the acoustic and optical modes. Each section is concluded by a discussion of the properties of the dispersion relation.

V. OVERLAPPED TRIANGULAR LATTICE

When the interaction between the two-components is attractive, it is energetically preferable to have the density minima of the two-components to coincide. However, if the intercomponent attraction is too strong there will be a

collapse type instability. This insight is validated by the calculations mentioned in Sec. II, where for $-1 < \alpha < 0$, the equilibrium lattice structure is triangular for both components and the vortex lattices of the two-components coincide. This overlapped triangular lattice is described by

$$u_* = 1/2, \qquad v_* = \sqrt{3}/2, \qquad a_* = b_* = 0. \tag{35}$$

The elastic energy in all the vortex lattices can be separated into two parts, elastic energy due to acoustic displacements ϵ_+, and elastic energy due to optical displacements ϵ_-. There will not be any terms that contain both, as such contributions to energy change sign under the exchange of components. So we can write

$$E_{\text{elastic}} = E^{\text{ac}}_{\text{elastic}} + E^{\text{op}}_{\text{elastic}}. \tag{36}$$

The acoustic contribution to the elastic energy will have the same form that is valid for a triangular lattice. In the LLL the hydrostatic compression modulus is zero and we need to consider only the shear modulus,

$$E^{\text{ac}}_{\text{elastic}} = \int d^2 r C^{\text{ac}} \left[\left(\frac{\partial \epsilon^x_+}{\partial x} - \frac{\partial \epsilon^y_+}{\partial y} \right)^2 + \left(\frac{\partial \epsilon^x_+}{\partial y} + \frac{\partial \epsilon^y_+}{\partial x} \right)^2 \right]. \tag{37}$$

Similarly, the only quadratic form one can make from ϵ_- which does not break the sixfold symmetry of the lattice is

$$E^{\text{op}}_{\text{elastic}} = \int d^2 r C^{\text{op}} \left(\vec{\epsilon}_- \right)^2. \tag{38}$$

The two elastic constants, C^{ac} and C^{op}, control the acoustic and optical Tkachenko modes, respectively. These two constants, however, have different dimensions, as is clear from their definition. We first nondimensionalize these constants as follows.

For the acoustic shear modulus, we can define a dimensionless quantity $\tilde{C}^{\text{ac}}$,

$$\tilde{C}^{\text{ac}} = \frac{C^{\text{ac}}}{gn^2}. \tag{39}$$

As explained in Sec. III, we can fit the energy near the minimum to a quadratic form,

$$E^{\text{ac}}_{\text{elastic}} = \frac{1}{2} gn^2 C_u \left[(u - u^*)^2 + (v - v_*)^2 \right], \tag{40}$$

which yields for the triangular lattice with $v_* = \sqrt{3}/2$

$$\tilde{C}^{\text{ac}} = \frac{3}{8} C_u. \tag{41}$$

The results of numerical calculation for C_u are displayed in Fig. 4. At $\alpha = 0$, the shear modulus for the acoustic modes takes the single-component value (per component) as expected from two noninteracting vortex lattices. As α is decreased towards -1, the shear modulus decreases linearly, signalling the collapse instability expected due to attractive interaction between the components.

Similarly the optical elastic constant can be nondimensionalized as

$$\tilde{C}^{\text{op}} = \frac{d^2}{gn^2} C^{\text{op}}, \tag{42}$$

where d is the lattice constant for the triangular lattice, which is related to rotation frequency as

$$d^2 = \frac{2\pi}{\sqrt{3} m \Omega}. \tag{43}$$

The optical part of the elastic energy can be fitted to the rotationally invariant form

$$E^{\text{op}}_{\text{elastic}} = \frac{gn^2}{2} C_{ab} [(a - a_*) + u_*(b - b_*)]^2 + [v_*(b - b_*)]^2. \tag{44}$$

which results in

$$\tilde{C}^{\text{op}} = \frac{1}{2} C_{ab}. \tag{45}$$

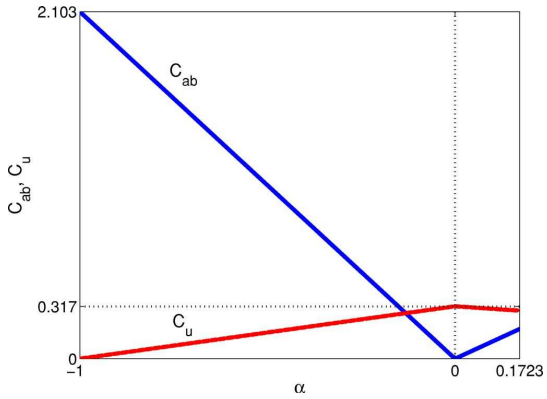

FIG. 4: Elastic constants (C_{ab}, C_u) of overlapped $(-1 < \alpha < 0)$ and interlaced $(0 < \alpha < 0.1723)$ triangular lattices with respect to α. As the attraction between the components increases $(\alpha \to -1)$, C_{ab} increases, and C_u decreases linearly. When there is no interaction between components $(\alpha = 0)$, $C_{ab} = 0$ which causes the discontinuity in the transition to interlaced triangular lattice. At $\alpha = 0$, the value of C_u is equal to the shear modulus of a one-component vortex lattice.

The result of numerical calculation for C_{ab} is plotted in Fig. 4. As α is decreased towards -1, it gets harder to separate the vortices of two-components, as expected from the increasing attraction between the components.

Once the elastic constants are known, the calculation of the Tkachenko modes for different lattices are straightforward, albeit tedious. In this section, we give a detailed calculation, while for all other lattice types we simply present the results of the calculation.

We first start with the calculation of the acoustic Tkachenko modes. With the form of the elastic energy given above, the acoustic stress is

$$\vec{\sigma}_+ = -4C^{\rm ac}\nabla^2\vec{\epsilon}_+. \tag{46}$$

Fourier transforming, we get $\vec{\sigma}_+ = 4C^{\rm ac}k^2\vec{\epsilon}_+$. Now, we also Fourier transform the polarization equation (32) to obtain

$$\epsilon_+^y = \frac{N_1}{D_1}\epsilon_+^x, \tag{47}$$

with

$$\begin{aligned} N_1 &= -i\omega k_y - 2\Omega k_x - \frac{2C^{\rm ac}}{mn\Omega}k^2k_x, \\ D_1 &= -i\omega k_x + 2\Omega k_y + \frac{2C^{\rm ac}}{mn\Omega}k^2k_y. \end{aligned} \tag{48}$$

Substituting the above result into Fourier transforms of Eqs. (33) and (34), we obtain

$$\left(\omega^2 - (1+\alpha)\frac{gn}{m}k^2\right)n_+ + n\left(4\Omega^2 + \frac{4C^{\rm ac}}{nm}k^2\right)\frac{\omega k^2}{D_1}\epsilon_+^x = 0 \tag{49}$$

and

$$-\frac{\omega^2}{n}n_+ + \left(\frac{4C^{\rm ac}}{nm}k^2 - \omega^2\right)\frac{\omega k^2}{D_1}\epsilon_+^x = 0. \tag{50}$$

By scaling the wave vector in frequency units,

$$k' = \sqrt{\frac{gn}{m}}k, \tag{51}$$

and using dimensionless elastic constants we obtain the characteristic equation as

$$\omega^4 - \omega^2\left[4\Omega^2 + (1+\alpha+8\tilde{C}^{\rm ac})k'^2\right] + (1+\alpha)4\tilde{C}^{\rm ac}k'^4 = 0. \tag{52}$$

This equation describes two different modes, one is a gapped sound mode, also called the inertial mode, while the other is the acoustic Tkachenko mode of the triangular lattice. To the lowest order in the long-wavelength approximation we get

$$\begin{aligned} \omega_I^{\rm ac} &= 2\Omega + \frac{1+\alpha+8\tilde{C}^{\rm ac}}{4\Omega}k'^2, \\ \omega_T^{\rm ac} &= \sqrt{(1+\alpha)\tilde{C}^{\rm ac}}\frac{k'^2}{\Omega}. \end{aligned} \tag{53}$$

The inertial mode is gapped, starting at 2Ω, and the second mode is the acoustic Tkachenko mode which has quadratic dispersion at long-wavelengths, similar to the Tkachenko mode in a one-component vortex lattice.

Calculation of the optical Tkachenko mode, similarly, starts by evaluating the optical part of the stress as

$$\vec{\sigma}_- = 4C^{\rm op}\vec{\epsilon}_-. \tag{54}$$

From the polarization equation we get

$$\epsilon_-^y = \frac{N_1}{D_1}\epsilon_-^x, \tag{55}$$

with

$$\begin{aligned} N_1 &= \omega k_y - i\left(2\Omega + \frac{2C^{\rm op}}{mn\Omega}\right)k_x \\ D_1 &= \omega k_x + i\left(2\Omega + \frac{2C^{\rm op}}{mn\Omega}\right)k_y \end{aligned} \tag{56}$$

which results in two coupled equations obtained from Eqs. (33) and (34)

$$\left(\omega^2 - (1-\alpha)\frac{gn}{m}k^2\right)n_- + n\left(4\Omega^2 + \frac{4C^{\rm op}}{mn}\right)i\frac{\omega k^2}{D_1}\epsilon_-^x = 0, \tag{57}$$

and

$$\frac{\omega^2}{n}n_- + \left[\omega^2 - \frac{2C^{\rm op}}{\Omega nm}\left(2\Omega + \frac{2C^{\rm op}}{\Omega nm}\right)\right]i\frac{\omega k^2}{D_1}\epsilon_-^x = 0. \tag{58}$$

Once again, using $k' = \sqrt{\frac{gn}{m}}k$, and the dimensionless elastic constants we obtain the dispersion relation for two modes,

$$\begin{aligned} \omega_I^{\rm op} &= 2\Omega\sqrt{1 + \frac{\sqrt{3}}{\pi}\tilde{C}^{\rm op}\frac{gn}{\Omega}} + \frac{1-\alpha}{4\Omega}k'^2, \\ \omega_T^{\rm op} &= \sqrt{\frac{\sqrt{3}}{2\pi}\tilde{C}^{\rm op}\frac{gn}{\Omega}}\,k'. \end{aligned} \tag{59}$$

These results are obtained to the lowest nonvanishing order in k' and also to the lowest order in $\frac{gn}{\Omega}$, which is a small parameter in the LLL regime.

The typical spectrum of the Tkachenko modes and the gapped sound modes are displayed in Fig. 5. The following properties of Tkachenko modes are revealed as a result of the above calculation.

First, we see that doubling the number of components in the BEC results in a doubling of the modes. Because the vortex lattice oscillations are coupled to density oscillations in a compressible fluid, there are four branches of excitation. The two inertial modes correspond to in-phase and out-of-phase oscillations of the densities of two-components and are gapped, starting essentially at twice the rotation frequency. As a second point, we find that the acoustic Tkachenko mode has quadratic k dependence at long-wavelength while the optical Tkachenko mode goes linearly with k. In an incompressible fluid, we would expect to find the acoustic modes with linear dispersion and the optical modes to be gapped. This result can be obtained by explicitly decoupling the density in the above calculation. Thus the extra factor of k in the dispersion is a result of the coupling between the density and the vortex lattice oscillations.

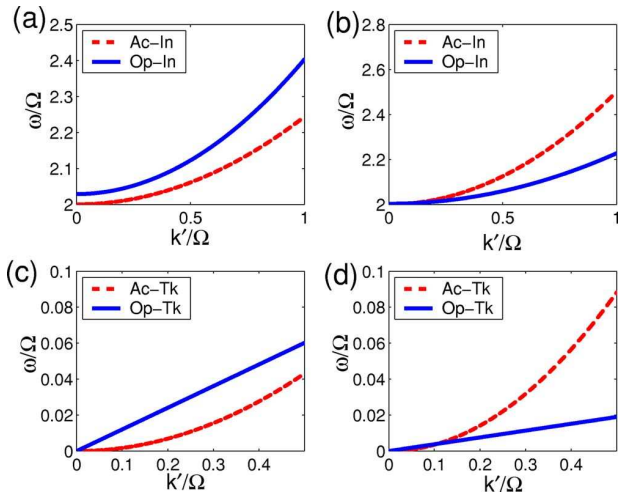

FIG. 5: Spectrum for overlapped triangular lattice, (a), (c), at $\alpha = -0.5$, and interlaced triangular lattice (b), (d) at $\alpha = 0.1$. k' and ω are scaled to rotation frequency Ω, and $\frac{gn}{\Omega} = 0.1$. Dispersion relations are the same for both lattice types, Eqs. (53) and (59). However, the elastic constants are different (see Fig. 4). Both acoustic and optical inertial modes, (a), (b), are gapped. For both lattices optical Tkachenko modes are linear while acoustic Tkachenko modes are quadratic in k.

While these two properties apply to all the lattice types considered below, there are some properties that are specific to the overlapped triangular lattice discussed in this section. First of all, the dispersion relation for both the optical and the acoustic Tkachenko modes are isotropic, i.e., independent of the direction of $\vec{k}$. The isotropy of the excitations is a direct consequence of the sixfold symmetry of the underlying lattice. The elastic (sound) waves in a triangular lattice also show isotropic behavior [26] and as we view the Tkachenko modes as the elastic excitations of the vortex lattice, this result is not unexpected. However, for the other, nontriangular, lattice types considered below, Tkachenko mode spectrum is anisotropic. A second property is revealed by investigating the behavior of the modes for changing α. As α goes to zero, the optical Tkachenko mode becomes softer and softer, revealing that the two lattices become mostly independent. Indeed at $\alpha = 0$ there is a first-order phase transition to the interlaced triangular lattice. As α approaches -1, this time it is the acoustic mode that becomes soft, and there is an instability towards collapse at exactly $\alpha = -1$. It is interesting to note that although our approach cannot describe this collapse, its signature is still present in the Tkachenko mode spectrum.

VI. INTERLACED TRIANGULAR LATTICE

For a single-component vortex lattice the equilibrium configuration is always the triangular lattice. When the interaction between the components of a two-component vortex lattice is weak, both vortex lattices stay triangular. The offset between the two-components is, however, decided by the sign of the intercomponent interaction. For attractive interaction $\alpha < 0$, the resulting lattice is the overlapped triangular lattice discussed in the previous section. For weak and repulsive interaction, it is energetically favorable to place the vortices of one-component at the density maxima of the other component. The resulting, interlaced triangular lattice is described by

$$u_* = \frac{1}{2}, \qquad v_* = \frac{\sqrt{3}}{2}, \qquad a_* = b_* = \frac{1}{3}. \tag{60}$$

The interlaced triangular lattice is the minimum-energy configuration for $0 < \alpha < 0.1724$, and is displayed in Fig. 1.

The elastic energy and the Tkachenko mode equations follow directly from the symmetry of the lattice. As the interlaced triangular lattice has exactly the same symmetry as the overlapped triangular lattice discussed in the previous section, the calculation given in the previous section is valid also for the interlaced triangular lattice. It is only the values of the elastic constants $\tilde{C}^{\rm ac}$ and $\tilde{C}^{\rm op}$, and their dependence on α, that is different from the previous case.

As a result, the acoustic modes are given by

$$\begin{aligned} \omega_I^{\rm ac} &= 2\Omega + \frac{1+\alpha+8\tilde{C}^{\rm ac}}{4\Omega}k'^2, \\ \omega_T^{\rm ac} &= \sqrt{(1+\alpha)\tilde{C}^{\rm ac}}\frac{k'^2}{\Omega} \end{aligned} \tag{61}$$

and the optical modes are given by

$$\begin{aligned} \omega_I^{\rm op} &= 2\Omega\sqrt{1+\frac{\sqrt{3}}{\pi}\tilde{C}^{\rm op}\frac{gn}{\Omega}} + \frac{1-\alpha}{4\Omega}k'^2, \\ \omega_T^{\rm op} &= \sqrt{\frac{\sqrt{3}}{2\pi}\tilde{C}^{\rm op}\frac{gn}{\Omega}}\,k'. \end{aligned} \tag{62}$$

Here the relations between $C^{\rm op}, C^{\rm ac}$ and C_u, C_{ab}, remain the same as in the previous section. A plot of the elastic constants is given in Fig. 4.

As in the previous section, we see that the acoustic Tkachenko mode is quadratic in k, at long-wavelengths, while the optical Tkachenko mode is linear in k. As a consequence of the sixfold symmetry of the underlying lattice, both modes are isotropic. A typical spectrum of the Tkachenko modes is displayed in Fig. 5. Just as the optical Tkachenko mode becomes soft for the overlapped triangular lattice as $\alpha = 0$ is approached from below, a similar softening takes place for the interlaced triangular lattice. So both sides of the first-order transition have dynamics characterized by a soft optical mode.

VII. SQUARE LATTICE

The lattice type which is energetically favorable over the largest range of intercomponent interaction is the square lattice. For $0.3733 < \alpha < 0.9256$, one-component's vortex lattice forms a square lattice while the other components vortices are situated at the centers of the squares (see Fig. 1). This lattice is characterized by

$$u_* = 0, \qquad v_* = 1, \qquad a_* = b_* = \frac{1}{2}. \tag{63}$$

For the square lattice we can write the elastic energy due to optical and acoustic deformations as

$$E_{\rm elastic} = E^{\rm ac}_{\rm elastic} + E^{\rm op}_{\rm elastic} \tag{64}$$

with

$$\begin{aligned} E^{\rm ac}_{\rm elastic} &= \frac{1}{2}\int d^2r \left[C_1^{\rm ac}\frac{\partial\epsilon_+^x}{\partial x}\frac{\partial\epsilon_+^y}{\partial y} + C_2^{\rm ac}\left(\frac{\partial\epsilon_+^x}{\partial y}+\frac{\partial\epsilon_+^y}{\partial x}\right)^2\right], \\ E^{\rm op}_{\rm elastic} &= \int d^2r C^{\rm op}\left(\vec{\epsilon}_-\right)^2. \end{aligned} \tag{65}$$

For acoustic modes we define the dimensionless elastic constants

$$\tilde{C}_1^{\rm ac} = \frac{C_1^{\rm ac}}{gn^2}, \qquad \tilde{C}_2^{\rm ac} = \frac{C_2^{\rm ac}}{gn^2}, \tag{66}$$

and fit the acoustic part of the elastic energy to the form

$$E^{\rm ac}_{\rm elastic} = \frac{gn^2}{2}\left[C_u(u-u_*)^2 + C_v(v-v_*)^2\right], \tag{67}$$

which yield

$$\tilde{C}_1^{\rm ac} = -4C_v, \qquad \tilde{C}_2^{\rm ac} = C_u. \tag{68}$$

The variation of elastic constants C_u and C_v are plotted in Fig. 6.

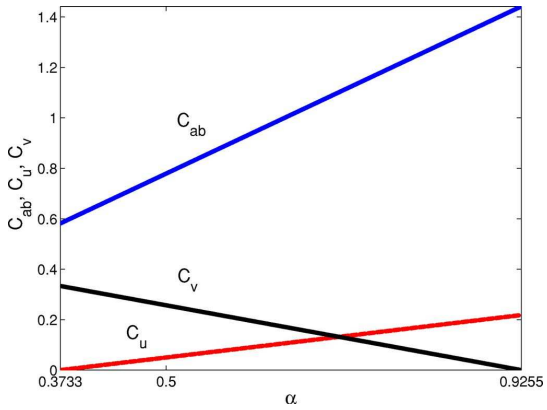

FIG. 6: Elastic constants (C_{ab}, C_u, C_v) of square lattice, Eqs. (67) and (75). As the components attract each other more, C_{ab} increases linearly. Both limits of α lead to second-order phase transitions. C_u and C_v vanish at $\alpha = 0.3733$ and $\alpha = 0.9255$, respectively.

The calculation of acoustic Tkachenko mode frequencies proceed similar to the previous sections. However, for the square lattice, the equations are not isotropic, for example the polarization equation (32) gives

$$\epsilon_+^y = \frac{N_1}{D_1}\epsilon_+^x, \tag{69}$$

with

$$\begin{aligned} N_1 &= \left(-i\omega k_y - 2\Omega k_x - \frac{4C_2^{\rm ac} + C_1^{\rm ac}}{2nm\Omega}k_x k_y^2\right), \\ D_1 &= \left(-i\omega k_x + 2\Omega k_y + \frac{4C_2^{\rm ac} + C_1^{\rm ac}}{2nm\Omega}k_y k_x^2\right). \end{aligned} \tag{70}$$

We find, in the long-wavelength limit, the inertial mode frequency

$$\omega_I^{\rm ac} = 2\Omega + \frac{1+\alpha+2\tilde{C}_2^{\rm ac}}{4\Omega}k'^2, \tag{71}$$

and the acoustic Tkachenko mode frequency

$$\omega_T^{\rm ac} = \sqrt{\frac{1+\alpha}{2}}\sqrt{\left[\tilde{C}_2^{\rm ac} f_2(\theta) - \tilde{C}_1^{\rm ac} f_1(\theta)\right]}\frac{k'^2}{\Omega}. \tag{72}$$

Here, we have

$$f_1(\theta) = \frac{1}{4}\sin^2(2\theta), \qquad f_2(\theta) = \cos^2(2\theta), \tag{73}$$

where θ is the angle from the $\hat{x}$ direction when the basis vectors of the vortex lattice are taken along $\hat{x}$ and $\hat{y}$.

For the optical spectrum, we define the dimensionless elastic constant

$$\tilde{C}^{\rm op} = \frac{d^2}{gn^2}C^{\rm op}, \tag{74}$$

where the lattice constant d is given by $d^2 = \frac{\pi}{\Omega m}$. The optical part of the elastic energy can be numerically fitted to a form

$$E_{\rm elastic}^{\rm op} = \frac{gn^2}{2}C_{ab}\left[(a-a_*)^2 + (b-b_*)^2\right], \tag{75}$$

which yields

$$\tilde{C}^{\rm op} = \frac{C_{ab}}{2}. \tag{76}$$

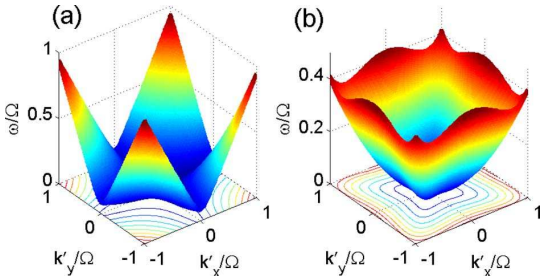

FIG. 7: Dispersion relation of the acoustic Tkachenko modes for the square lattice, Eq. (72) for $\alpha = 0.4$ (a), and $\alpha = 0.85$ (b). Underlying contour plots are given to illustrate the anisotropy of the modes.

The dependence of the elastic constant C_{ab} on α is plotted in Fig. 6.

The gapped inertial mode and the optical Tkachenko mode are calculated to the lowest order in k' and $\frac{gn}{\Omega}$ as

$$(\omega_I^{\rm op})^2 = 4\Omega^2 \left[1 + \frac{2gn}{\pi\Omega}\tilde{C}^{\rm op}\right] + (1-\alpha)k'^2, \tag{77}$$

and

$$\omega_T^{\rm op} = \sqrt{\frac{1-\alpha}{\pi + 2\frac{gn}{\Omega}\tilde{C}^{\rm op}}}\sqrt{\frac{gn}{\Omega}\tilde{C}^{\rm op}}\, k', \tag{78}$$

respectively.

The above results reveal a number of properties of the Tkachenko modes of a square vortex lattice. Similar to the triangular lattice, there are two gapped modes, which are the sound modes of the two-component condensate modified by the interactions with the vortex oscillations. The remaining two gapless modes are the acoustic Tkachenko mode and the optical Tkachenko mode, which have k^2 and k dispersion, respectively. Both the two gapped modes and the optical Tkachenko mode have isotropic behavior, however, the underlying square lattice causes the acoustic Tkachenko mode dispersion to be anisotropic. The anisotropy of the acoustic Tkachenko mode is more transparent when written as

$$\omega_T^{\rm ac} = \sqrt{2(1+\alpha)\left[C_u\cos^2(2\theta) + C_v\sin^2(2\theta)\right]}\frac{k'^2}{2\Omega}. \tag{79}$$

The acoustic mode spectrum is plotted in Fig. 7 for two different values of α. We notice that depending on the elastic constants two different types of softening happens for the acoustic Tkachenko modes. If $C_u = 0$, then the acoustic modes along the directions

$$\theta = 0, \pi/2, \pi, 3\pi/2 \tag{80}$$

become soft. We see from the numerical fit that C_u becomes zero near $\alpha = 0.3733$ and these soft modes control the dynamics of the second-order phase transition to the rhombic lattice. The other possibility for soft mode formation is when $C_v = 0$. In this case the soft acoustic modes are along the directions

$$\theta = \pi/4, 3\pi/4, 5\pi/4, 7\pi/4. \tag{81}$$

These soft modes, then, signal the second-order phase transition to the rectangular lattice, at $\alpha = 0.9256$.

VIII. RECTANGULAR LATTICE

When the interactions between the components are close to the interactions within each component, the energetically favorable lattice becomes a rectangular lattice. The rectangular lattice has $a_* = b_* = 1/2$, so vortices of one-component are placed at the centers of the rectangles formed by the vortices of the other component. The ratio of the long side of the rectangles to their short side, v_*, increases with increasing α (see Fig. 2).

The elastic energy can once again be separated as

$$E_{\rm elastic} = E^{\rm ac}_{\rm elastic} + E^{\rm op}_{\rm elastic}. \tag{82}$$

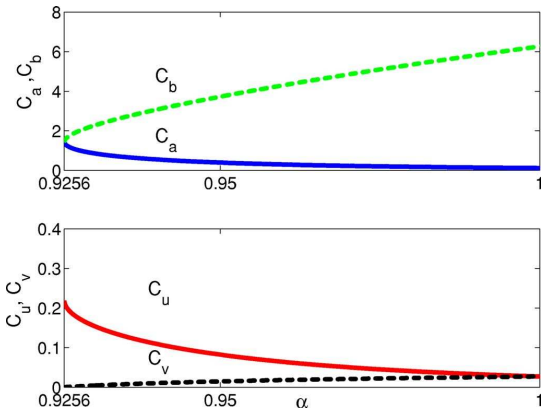

FIG. 8: Elastic constants (C_a, C_b, C_u, C_v) of rectangular lattice. The upper figure shows optical elastic constants(C_a, C_b). As $\alpha \to 1$, C_a vanishes. The lower figure shows acoustic elastic constants (C_u, C_v). As $\alpha \to 1$, $C_u \to C_v$ and there remains only one acoustic elastic constant similar to the one-component triangular lattice.

Here, we express the acoustic part of the elastic energy as

$$E^{\rm ac}_{\rm elastic} = \frac{1}{2}\int d^2r \left[C^{\rm ac}_1 \left(\frac{\partial \epsilon^x_+}{\partial x} - \frac{\partial \epsilon^y_+}{\partial y}\right)^2 + C^{\rm ac}_2 \left(\frac{\partial \epsilon^x_+}{\partial y} + \frac{\partial \epsilon^y_+}{\partial x}\right)^2\right], \tag{83}$$

a form that is essentially the same as the square lattice, as the hydrostatic compression modulus is zero. The optical part is

$$E^{\rm op}_{\rm elastic} = \int d^2r \left[C^{\rm op}_1 \left(\epsilon^x_-\right)^2 + C^{\rm op}_2 \left(\epsilon^y_-\right)^2\right]. \tag{84}$$

For the acoustic modes, we define the dimensionless elastic constants

$$\tilde{C}^{\rm ac}_1 = \frac{C^{\rm ac}_1}{gn^2}, \qquad \tilde{C}^{\rm ac}_2 = \frac{C^{\rm ac}_2}{gn^2}, \tag{85}$$

and fit the acoustic part of the elastic energy to the form

$$E^{\rm ac}_{\rm elastic} = \frac{gn^2}{2}\left[C_u(u-u_*)^2 + C_v(v-v_*)^2\right], \tag{86}$$

which results in

$$\tilde{C}^{\rm ac}_1 = v_*^2 C_v, \qquad \tilde{C}^{\rm ac}_2 = v_*^2 C_u. \tag{87}$$

The numerical results for elastic constants C_u and C_v are given in Fig. 8.

As a result, we calculate the acoustic Tkachenko mode frequency

$$\omega^{\rm ac}_T = \sqrt{\frac{1+\alpha}{2}}\sqrt{\tilde{C}^{\rm ac}_1 \sin^2(2\theta) + \tilde{C}^{\rm ac}_2 \cos^2(2\theta)}\frac{k'^2}{\Omega}, \tag{88}$$

and the acoustic inertial mode frequency

$$(\omega^{\rm ac}_I)^2 = 4\Omega^2 + [1+\alpha+2(\tilde{C}^{\rm ac}_1 + \tilde{C}^{\rm ac}_2)]k'^2. \tag{89}$$

For the optical modes, we nondimensionalize

$$\tilde{C}^{\rm op}_1 = \frac{d_1^2}{gn^2}C^{\rm op}_1, \qquad \tilde{C}^{\rm op}_2 = \frac{d_2^2}{gn^2}C^{\rm op}_2, \tag{90}$$

where d_1 and d_2 are the sides of the rectangular unit cell with

$$d_1^2 = \frac{\pi}{\Omega m v_*}, \qquad d_2^2 = \frac{\pi v_*}{\Omega m}. \tag{91}$$

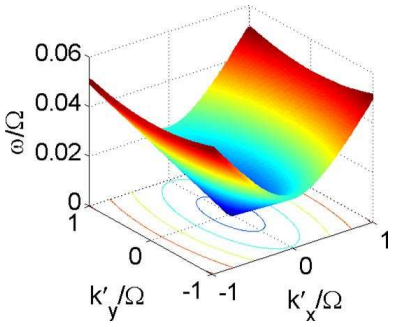

FIG. 9: Dispersion relation of the optical Tkachenko mode of the rectangular lattice, Eq. (94), for $\alpha = 0.95$, $\frac{gn}{\Omega} = 0.1$. The underlying contour plot reflects the symmetry of the rectangular lattice.

When the elastic energy is fitted to the numerical form

$$E^{\rm op}_{\rm elastic} = \frac{gn^2}{2}\left[C_a(a-a_*)^2 + C_b(b-b_*)^2\right], \tag{92}$$

we obtain

$$\tilde{C}^{\rm op}_1 = \frac{C_a}{2}, \qquad \tilde{C}^{\rm op}_2 = \frac{C_b}{2}, \tag{93}$$

The dependence of C_a and C_b on α is plotted in Fig. 8.

As a result of the calculation, we obtain the optical Tkachenko mode dispersion

$$\omega^{\rm op}_T = \sqrt{\frac{1-\alpha}{\pi}\frac{gn}{\Omega}}\sqrt{\frac{\tilde{C}^{\rm op}_2}{v_*}\cos^2(\theta) + \tilde{C}^{\rm op}_1 v_* \sin^2(\theta)}\, k', \tag{94}$$

and the inertial mode frequencies

$$(\omega^{\rm op}_I)^2 = 4\Omega^2\left[1 + \frac{gn}{\pi\Omega}\left(v_*\tilde{C}^{\rm op}_1 + \frac{1}{v_*}\tilde{C}^{\rm op}_2\right)\right] + (1-\alpha)k'^2. \tag{95}$$

A number of important conclusions can be deduced from the above results. First of all, both the acoustic and optical Tkachenko modes are anisotropic, while the inertial modes are isotropic for the rectangular lattice. While the anisotropy of the acoustic Tkachenko mode, is similar to the anisotropy obtained for the square lattice, the anisotropy of the optical modes can be understood by a different mechanism. The rectangular lattice can be thought of as alternating planes of vortices of different components. It is easier to move the vortices in these planes, rather than perpendicular to these planes. A typical dispersion of optical Tkachenko modes is given in Fig. 9.

As a second property, we see that near $\alpha = 0.9256$ there is a soft acoustic mode, signaling a second-order transition to the square lattice. Thus both sides of the transition from square to rectangular lattice have a soft acoustic mode.

When intercomponent interaction is equal in strength to the interaction within the components, i.e., $\alpha = 1$, a number of interesting phenomena are expected. First, at $\alpha = 1$, there is no distinction between different components, and one would expect the results to be the same as that of a single-component vortex lattice. Indeed, at this point, $v_* = \sqrt{3}$, and the resulting rectangular lattice is equivalent to a single-component triangular lattice. Furthermore, the acoustic mode spectrum becomes isotropic exactly at this point, as can be seen in Fig. 10.

However, the point $\alpha = 1$, where the intercomponent interaction is the same as the interaction between the components, is special in another way. For a nonrotating two-component BEC, there is an instability towards phase-separation at this point. In previous studies of two-component BECs with vortex lattices, this instability was not observed. However, we find that at $\alpha = 1$ the optical Tkachenko mode becomes soft, and the system is unstable beyond $\alpha = 1$. This is reflected in the $\sqrt{1-\alpha}$ term, in the dispersion relation Eq. (94). Thus we find that there is an instability beyond $\alpha = 1$, for rapidly rotating two-component condensates. As previous studies of this system did not take the coupling between the vortex movement and density oscillations into account, it is not surprising that this instability was not observed.

Although we find that there is an instability at $\alpha = 1$, it is not clear that this instability leads directly to phase-separation. The analog of the sound mode that is unstable in a nonrotating system is the optical inertial mode. As this mode has a gap, there is no instability in the long-wavelength. We find that the dispersion of the optical inertial

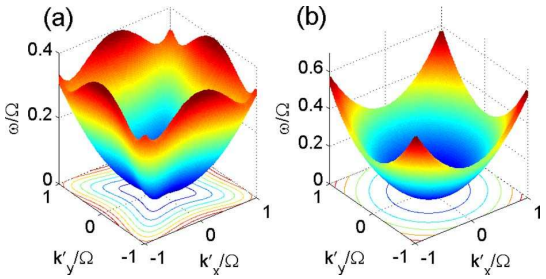

FIG. 10: Dispersion relation of the acoustic Tkachenko modes of the rectangular lattice, Eq. (88) for $\alpha = 0.95$ (a) and for $\alpha = 1.0$ (b). At $\alpha = 1.0$, the dispersion relation becomes isotropic. The similarity between (a) and Fig. 7(b) is due to the second-order phase transition between square and rectangular lattices.

mode has a k^2 term with a negative coefficient, but this is not sufficient to claim that there will be an instability at a finite value of k, as higher-order terms such as k^4 may prevent the dispersion from reaching zero frequency. Instead there may be a phase with partial phase-separation and disordered distribution of vortices beyond $\alpha = 1$. Further investigation of this instability is needed to determine the nature of the phase beyond $\alpha = 1$.

IX. RHOMBIC LATTICE

The final lattice type we consider is the rhombic lattice, which is the minimum-energy configuration for $0.1724 < \alpha < 0.3733$. This lattice is an intervening phase between the interlaced triangular lattice and the square lattice discussed in previous sections. At $\alpha = 0.1724$ there is a first-order transition from the interlaced triangular lattice, where a_* and b_* change discontinuously from $1/2$ to

$$a_* = b_* = \frac{1}{3}. \tag{96}$$

The unit cell also becomes a rhombus, while the acute angle of the rhombus η continuously changes from 67.96° to 90°. A plot of the lattice geometry and the change of η is given in Fig. 2.

The rhombic lattice has twofold (reflection) symmetry along the axis that makes an angle $\eta/2$ with the primitive basis vectors. However, instead of expressly taking advantage of this symmetry, we use a general form for the elastic energy. Writing

$$E_{\text{elastic}} = E^{\text{ac}}_{\text{elastic}} + E^{\text{op}}_{\text{elastic}}, \tag{97}$$

we use

$$E^{\text{ac}}_{\text{elastic}} = \frac{1}{2}\int d^2r \left[C_1^{\text{ac}} \left(\frac{\partial \epsilon_+^x}{\partial x} - \frac{\partial \epsilon_+^y}{\partial y} \right)^2 + C_2^{\text{ac}} \left(\frac{\partial \epsilon_+^x}{\partial y} + \frac{\partial \epsilon_+^y}{\partial x} \right)^2 + C_3^{\text{ac}} \left(\frac{\partial \epsilon_+^x}{\partial y} + \frac{\partial \epsilon_+^y}{\partial x} \right) \left(\frac{\partial \epsilon_+^x}{\partial x} - \frac{\partial \epsilon_+^y}{\partial y} \right) \right], \tag{98}$$

and

$$E^{\text{op}}_{\text{elastic}} = \int d^2r \left[C_1^{\text{op}} \left(\epsilon_-^x \right)^2 + C_2^{\text{op}} \left(\epsilon_-^y \right)^2 + C_3^{\text{op}} \epsilon_-^x \epsilon_-^y \right]. \tag{99}$$

For the acoustic modes, we define dimensionless quantities

$$\tilde{C}_1^{\text{ac}} = \frac{C_1^{\text{ac}}}{gn^2}, \qquad \tilde{C}_2^{\text{ac}} = \frac{C_2^{\text{ac}}}{gn^2}, \qquad \tilde{C}_3^{\text{ac}} = \frac{C_3^{\text{ac}}}{gn^2}, \tag{100}$$

and fit the acoustic part of the elastic energy to the form

$$E^{\text{ac}}_{\text{elastic}} = \frac{gn^2}{2} \left[C_u (u - u_*)^2 + C_v (v - v_*)^2 + C_{uv} (u - u_*)(v - v_*) \right], \tag{101}$$

which yields

$$\tilde{C}_1^{\text{ac}} = v_*^2 C_v, \qquad \tilde{C}_2^{\text{ac}} = v_*^2 C_u, \qquad \tilde{C}_3^{\text{ac}} = -v_*^2 C_{uv}. \tag{102}$$

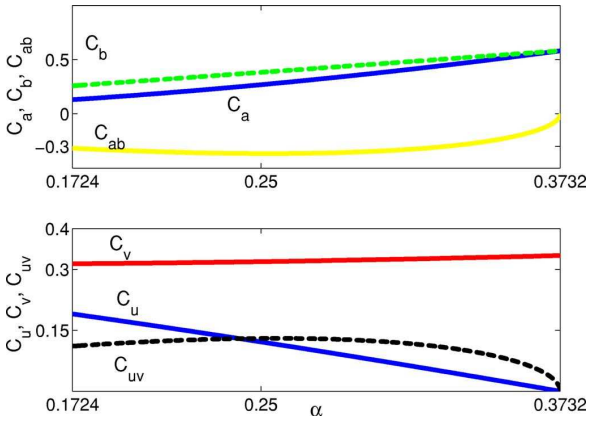

FIG. 11: Optical elastic constants [upper, Eq. (108)] and acoustic elastic constants [lower, Eq. (101)] of rhombic lattice with respect to α. As $\alpha \to 0.3732$, $C_a \to C_b$, and C_u, C_v vanish, leaving two optical elastic constants, and one acoustic elastic constant for the square lattice. In the opposite limit $\alpha \to 0.1724$, six elastic constants remain due to the discontinuity in the transition to interlaced triangular lattice.

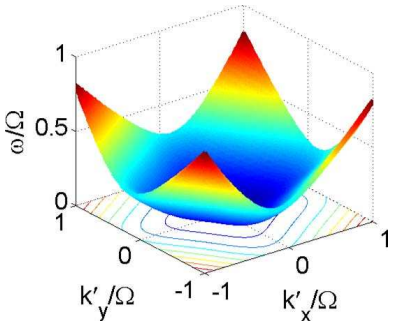

FIG. 12: Dispersion relation of the acoustic Tkachenko mode of the rhombic lattice, Eq. (104), for $\alpha = 0.2$. The anisotropy reflects the twofold symmetry of the rhombic lattice (see Fig. 13).

The numerical results for elastic constants C_u, C_v, and C_{uv} are given in Fig. 11.

We find the acoustic inertial mode dispersion

$$(\omega_I^{\rm ac})^2 = 4\Omega^2 + [1 + \alpha + 2(\tilde{C}_1^{\rm ac} + \tilde{C}_2^{\rm ac})]k'^2, \tag{103}$$

and the acoustic Tkachenko mode dispersion

$$\omega_T^{\rm ac} = \sqrt{\frac{1+\alpha}{2}}\sqrt{4\tilde{C}_1^{\rm ac}\frac{k_x^2 k_y^2}{k^4} + \tilde{C}_2^{\rm ac}\frac{(k_x^2-k_y^2)^2}{k^4} + 2\tilde{C}_3^{\rm ac}\frac{k_x k_y (k_y^2-k_x^2)}{k^4}}\,\frac{k'^2}{\Omega}. \tag{104}$$

The anisotropy of the Tkacheko mode is more transparent when represented in terms of θ, the angle from the $\hat{x}$ axis,

$$\omega_T^{\rm ac} = \sqrt{\frac{1+\alpha}{2}}\sqrt{\tilde{C}_1^{\rm ac}\sin^2(2\theta) + \tilde{C}_2^{\rm ac}\cos^2(2\theta) - \tilde{C}_3^{\rm ac}\sin(4\theta)}\,\frac{k'^2}{\Omega}. \tag{105}$$

For the optical modes, we define the dimensionless elastic constants,

$$\tilde{C}_1^{\rm op} = \frac{d^2}{gn^2}C_1^{\rm op}, \qquad \tilde{C}_2^{\rm op} = \frac{d^2}{gn^2}C_2^{\rm op}, \qquad \tilde{C}_3^{\rm op} = \frac{d^2}{gn^2}C_3^{\rm op}, \tag{106}$$

where the side length of the rhombus d is

$$d^2 = \frac{\pi}{\Omega m \sin(\eta)}. \tag{107}$$

We use a numerical fit to the energy of the general form

$$E_{\rm elastic}^{\rm op} = \frac{gn^2}{2}\left\{C_{ax}[(a-a_*) + u_*(b-b_*)]^2 + C_{by}v_*^2(b-b_*)^2 + C_{ab}[(a-a_*) + u_*(b-b_*)]v_*(b-b_*)\right\}, \tag{108}$$

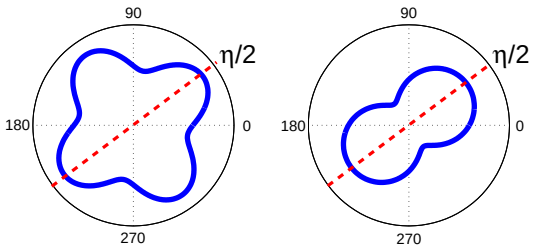

FIG. 13: Polar plot of the frequency of the acoustic [left, Eq. (104)] and the optical [right, Eq. (111)] Tkachenko modes for the rhombic lattice ($k = 0.1$, $\frac{gn}{\Omega} = 0.1$, $\alpha = 0.2$). $\eta/2$ is the opening angle of the rhombic unit cell at $\alpha = 0.2$.

which yields

$$\tilde{C}_1^{\rm op} = \frac{C_{ax}}{2}, \qquad \tilde{C}_2^{\rm op} = \frac{C_{by}}{2}, \qquad \tilde{C}_3^{\rm op} = \frac{C_{ab}}{2}, \tag{109}$$

The dependence of C_{ax}, C_{by}, and C_{ab} on α is plotted in Fig. 11.

We find the optical inertial mode

$$(\omega_I^{\rm op})^2 = 4\Omega^2 \left[1 + \frac{gn}{\pi\Omega}\sin(\eta)\left(\tilde{C}_1^{\rm op} + \tilde{C}_2^{\rm op}\right)\right] + (1-\alpha)k'^2, \tag{110}$$

and the optical Tkachenko mode

$$\omega_T^{\rm op} = \sqrt{\frac{1-\alpha}{\pi}\frac{gn}{\Omega}\sin(\eta)}\sqrt{\tilde{C}_2^{\rm op}\cos^2(\theta) + \tilde{C}_1^{\rm op}\sin^2(\theta) - \frac{1}{2}\tilde{C}_3^{\rm op}\sin(2\theta)}\,k'. \tag{111}$$

For the rhombic lattice, both the acoustic and the optical Tkachenko modes are anisotropic. A typical dispersion for the acoustic Tkachenko modes is displayed in Fig. 12. In the calculation above we have not implicity assumed the twofold symmetry of the rhombic lattice, however, the resulting dispersion relations respect this symmetry. As an example the polar plot of optical and acoustic mode frequencies is given in Fig. 13. This symmetry can be viewed as a validation of the numerical approach we use to calculate the elastic coefficients.

Another property of the Tkachenko modes of the rhombic lattice is that the transition to the square lattice at $\alpha = 0.3733$ is accompanied by a soft acoustic mode. However, the first-order transition to the triangular lattice does not have any soft acoustic or optical Tkachenko mode.

X. STRUCTURAL PHASE TRANSITIONS

The two-component vortex lattice system has five different equilibrium lattice types and four structural phase transitions between them. In this section, we comment on the interplay between these transitions and the Tkachenko modes of the lattice. Our aim is to give an overall picture of the physics in this system as the intercomponent interaction α is varied. We start from $\alpha = -1$, and consider all transitions as α is increased.

For $\alpha < -1$, the two-component BEC system is unstable towards collapse due to the strength of attraction between the components. This instability is apparent in the Tkachenko mode spectrum of the overlapped triangular lattice for α values greater than but close to -1. Here there is a soft acoustic Tkachenko mode, as discussed in Sec. V.

At $\alpha = 0$, when there is no interaction between the two-components of the BEC, the vortex lattice geometry changes from overlapped triangular lattice to the interlaced triangular lattice. This first-order transition leaves the unit cell geometry the same, however, there is a discontinuous jump in the relative positions of vortices within the unit cell. On both sides of the transition there is a soft optical Tkachenko mode. Thus the reordering inside the unit cell is accompanied by a soft long-wavelength mode as expected.

As the intercomponent repulsion is increased further, there is a first-order phase transition from the interlaced triangular lattice to the rhombic lattice, at $\alpha = 0.1724$. In this transition, both the unit cell geometry and the positions of vortices inside the unit cell change discontinuously. We find no signature of this transition in the long-wavelength optical or acoustic modes. The instability mechanism causing this transition must include both optical and acoustic Tkachenko modes, and must take place at wavelengths comparable to the lattice spacing. Thus this instability is not captured by our linear, long-wavelength approach.

Between $\alpha = 0.1724$ and $\alpha = 0.3733$ the rhombic lattice is the minimum-energy configuration, and at $\alpha = 0.3733$ there is a second-order phase transition to the square lattice. On both sides of this transition there is a soft acoustic Tkachenko mode. The acoustic modes have anisotropic dispersion for both square and rhombic lattices, and the soft mode has a wave vector $\vec{k}$, that is parallel to the primitive lattice basis vectors $\vec{a}_1 = d\hat{x}$, or $\vec{a}_2 = d\hat{y}$. As in the structural phase transitions of solids, a second-order phase transition is accompanied by a soft acoustic mode.

The final structural phase transition between different lattice geometries takes place at $\alpha = 0.9256$, between the square and rectangular lattices. This is a second-order phase transition, and we find that there is a soft acoustic Tkachenko mode on both sides of the transition. The soft mode has a wave vector $\vec{k}$ that makes an angle of $\pi/4$ with the primitive lattice basis vectors, $\vec{k} \parallel (\vec{a}_1 + \vec{a}_2)$.

For a nonrotating system there is a phase-separation instability at $\alpha = 1$. We find that at this point the optical Tkachenko modes of the rotating system become soft. However, as discussed in Sec. VIII, it is not clear if this instability directly leads to phase-separation, or to another phase.

XI. CONCLUSION

We conclude by giving a summary of our main results and discuss their relevance to the recent experiment on the vortex lattice of the two-component rubidium BEC.

We considered a rapidly rotating two-component BEC, and calculated the Tkachenko mode dispersion relations for different lattice geometries. We find that a two-component vortex lattice has two branches of Tkachenko modes, which we call acoustic and optical Tkachenko modes in analogy with phonons. The acoustic Tkachenko modes have k^2 dispersion at long-wavelengths while the optical Tkachenko modes have linear, k, dispersion. For all lattice types other than triangular lattices, the dispersion relations are anisotropic. By investigating the behavior of Tkachenko modes near structural phase transitions, we identified the soft modes that are responsible for the phase transitions. Out of the four structural phase transitions two are of second-order, while the remaining two are first-order. The second-order transitions are accompanied by the softening of an acoustic mode. For one of the first-order phase transitions we identified a soft optical Tkachenko mode, while for the other first-order transition, no such long-wavelength mode was found. We also found that if the intercomponent repulsion is stronger than the interactions within each component, the vortex lattice is unstable. This instability may lead to phase-separation, as is the case for a nonrotating two-component BEC.

In a recent experiment at JILA [23], a rapidly rotating two-component Rb condensate was created. It was found that the equilibrium vortex lattice configuration is square. Furthermore, when the lattice was perturbed, a Tkachenko like mode was observed, however, this mode was found to be heavily damped, thus it has not been possible to measure the Tkachenko mode frequencies.

There are three important points to consider when comparing our results with this experiment. First the interaction parameters for the Rb system used in the experiment are different from what was considered in this paper, most importantly, interaction parameters within each component are not the same,

$$g_{11} \neq g_{22}. \tag{112}$$

In this case, one would expect the acoustic and optical Tkachenko modes to be coupled. However, this coupling should be relatively small, as

$$\frac{2(g_{11} - g_{22})}{g_{11} + g_{22}} \approx 0.05. \tag{113}$$

When the interaction strengths within each component is different, we may redefine

$$\alpha = \frac{g_{12}}{\sqrt{g_{11} g_{22}}}, \tag{114}$$

which for the Rb system is very close to 1. Although the calculations in the LLL indicate that a rectangular lattice is more favorable, experimentally the lattice structure is found to be a square within experimental error. This implies, as a second point, that one must take into account that the experimental system is not fully in the LLL regime. As the third and final point, the experimental system is of finite extent. The overall density profile in the system is affected by the finite size of the system and may cause in shifts in vortex positions [28]. More importantly, the coupling between vortex oscillations and the density modes, coupled with other loss mechanisms, damp the Tkachenko modes.

The above limitations prevent a direct quantitative comparison of data with the theory presented in this paper. There are, however, some important qualitative conclusions that can be drawn. A puzzling result of the experiment is

that the Tkachenko excitations in the two-component BEC are more heavily damped compared to a single-component system. It is thought that the main damping mechanism is the coupling to surface modes near the edges of the cloud, but this mechanism would be independent of whether one is using a one-component or a two-component condensate. We believe that there are two effects that contribute to this apparently high damping rate. The method used in the experiment to excite Tkachenko modes is to focus a resonant laser beam onto the center of the condensate. This method excites Tkachenko modes isotropically, giving equal weight to every direction. However, our calculations show that Tkachenko modes in a square (or rectangular) lattice are anisotropic. This anisotropy is very pronounced if the system is close to square to rectangular structural phase transition, which the experimental system could be as indicated by the ratio of its interaction strengths. When Tkachenko modes are excited isotropically, because oscillations along different directions have different frequencies, there will be a significant dephasing effect. We believe a significant part of the observed damping is due to this dephasing. A second effect is that, because of the coupling between the acoustic and the optical modes, during the excitation also optical Tkachenko modes are excited. By making measurements on the vortex positions of one-component it is not possible to distinguish one type of oscillation from the other. We believe, if the excitation mechanism can be made anisotropic, for example by using a resonant laser with an elliptical focus, it should be possible to observe smaller damping rates.

It is also interesting to note that it should be possible to measure optical Tkachenko modes, using the same interference technique used in the experiment to prove that the vortices form interlaced lattices. An optical Tkachenko mode, once excited, would cause oscillations in the visibility of the obtained "vortex lattice interference" fringes.

Acknowledgments

This work was supported by TUBITAK-KARIYER Grant No. 104T165 and a TUBA-GEBIP grant. M.Ö. Oktel would like to thank Erich Mueller for useful discussions and Aspen Center for Physics for their hospitality.

[1] A. A. Abrikosov, Zh. Éksp. Teor. Fiz. **32**, 1442 (1957) [Sov. Phys. JETP **5**, 1174 (1957)].
[2] H. Träuble and U. Essmann, Phys. Lett. **24A**, 526 (1967).
[3] E. J. Yarmchuck and R. E. Packard, J. Low Temp. Phys. **46**, 479 (1982).
[4] J. R. Abo-Shaeer, C. Raman, J. M. Vogels, and W. Ketterle, Science **292**, 476 (2001).
[5] P. C. Haljan, I. Coddington, P. Engels, and E. A. Cornell, Phys. Rev. Lett. **87**, 210403 (2001).
[6] M. W. Zwierlein, J. R. Abo-Shaeer, A. Schirotzek, C. H. Schunck, and W. Ketterle, Nature (London), **435**, 1047 (2005).
[7] V. K. Tkachenko, Zh. Éksp. Teor. Fiz. **49**, 1875 (1965) [Sov. Phys. JETP **22**, 1282 (1966)]; **50**, 1573 (1966) [**23**, 1049 (1966)]; **56**, 1763 (1969) [**29**, 945 (1969)].
[8] G. Baym, and E. Chandler, J. Low Temp. Phys. **50**, 57 (1983); **62**, 119 (1986); E. B. Sonin, Zh. Éksp. Teor. Fiz. **70**, 1970 (1976) [Sov. Phys. JETP **43**, 1027 (1976)]; M. R. Williams and A. L. Fetter, Phys. Rev. B **16**, 4846, (1977).
[9] J. Sinova, C. B. Hanna, and A. H. MacDonald, Phys. Rev. Lett. **89**, 030403 (2002).
[10] M. Ruderman, Nature (London) **225**, 619 (1970).
[11] I. Coddington, P. Engels, V. Schweikhard, and E. A. Cornell, Phys. Rev. Lett. **91**, 100402 (2003).
[12] J. R. Anglin and M. Crescimanno, cond-mat/0210063.
[13] G. Baym, Phys. Rev. Lett. **91**, 110402 (2003).
[14] E. B. Sonin, Phys. Rev. A **72**, 021606(R) (2005).
[15] M. Cozzini, S. Stringari, and C. Tozzo, cond-mat/0509559.
[16] E. B. Sonin, Phys. Rev. A **71**, 011603(R) (2005).
[17] M. Cozzini, L. P. Pitaevskii, and S. Stringari, Phys. Rev. Lett. **92**, 220401 (2004).
[18] L. O. Baksmaty, S. J. Woo, S. Choi, and N. P. Bigelow, Phys. Rev. Lett. **92**, 160405 (2004).
[19] T. Mizushima, Y. Kawaguchi, K. Machida, T. Ohmi, T. Isoshima, and M. M. Salomaa, Phys. Rev. Lett. **92**, 060407 (2004).
[20] T.-L. Ho, Phys. Rev. Lett. **87**, 060403 (2001).
[21] N. R. Cooper, N. K. Wilkin, and J. M. F. Gunn, Phys. Rev. Lett. **87**, 120405 (2001).
[22] V. Schweikhard, I. Coddington, P. Engels, V. P. Mogendorff, and E. A. Cornell, Phys. Rev. Lett. **92**, 040404 (2004).
[23] V. Schweikhard, I. Coddington, P. Engels, S. Tung, and E. A. Cornell, Phys. Rev. Lett. **93**, 210403 (2004).
[24] E. J. Mueller and T-L. Ho, Phys. Rev. Lett. **88**, 180403 (2002).
[25] K. Kasamatsu, M. Tsubota, and M. Ueda, Phys. Rev. Lett. **91**, 150406 (2003).
[26] L. D. Landau and E. M. Lifshitz, *Theory of Elasticity*, (Pergamon, Oxford, 1970), pp. 35-37.
[27] C. Kittel, *Introduction to Solid State Physics*, 7th edition, (Jonh Wiley & Sons, New York, 1996), p. 402.
[28] G. Baym and C. J. Pethick, Phys. Rev. A **69**, 043619 (2004).